

## Morphology of Polyethylene Crystallized Under the Simultaneous Influence of Pressure and Orientation in a Capillary Viscometer

RICHARD G. CRYSTAL, *Rochester Research Laboratories, Xerox Corporation, Rochester, New York 14603*, and JOHN H. SOUTHERN,\* *Polymer Science and Engineering, University of Massachusetts, Amherst, Massachusetts 01002*

### Synopsis

The morphology of high-density polyethylene crystallized under simultaneous pressure and shear in an Instron capillary viscometer has been examined by scanning electron microscopy, electron microscopy, and selected-area electron diffraction. Two distinct fibrous morphologies were observed in these unusually transparent strands. The outer sheath was composed of fibers, 3000 Å in diameter, aligned parallel to the extrusion direction and apparently interconnected by a lamellar cross texture. A highly crystalline ribbon texture composed of fine fibers, 200–250 Å in diameter, dominated the inner core. Sharp-spot electron diffraction patterns obtained from these central ribbons indicated a high degree of *c*-axis orientation parallel to the fibers and an extended-chain crystal structure. The melting behavior of both irradiated and unirradiated strands examined by differential scanning calorimetry was consistent with the formation of two distinct crystalline morphological units.

### INTRODUCTION

The morphologies of linear polyethylene crystallized from the melt under high pressure and crystallized under shear from both the melt and dilute solution have been reported previously. Wunderlich and others<sup>1-6</sup> have described the extended-chain structure crystallized under static pressures of at least 300 atm. The morphology so produced is characterized by striated, extended-chain crystals in which the molecular axis is oriented parallel to the striations. Pennings and others<sup>7-9</sup> have demonstrated that a fibrous morphology is generated when, for example, a dilute solution of polyethylene (1% in xylene) is stirred during crystallization. Electron microscopy has shown that the individual fibers crystallized under these shearing conditions contain chain-folded lamellae attached to an extended chain central backbone, resulting in a "shishkabob" arrangement. Furthermore, Keller and Hill<sup>10,11</sup> have shown that an analogous, fibrous crystalline structure can be generated when a lightly cross-linked polyethylene is

\* Present address: Technical Center, Monsanto Company, Pensacola, Florida 32502.

cooled from the melt under stress. They reported extensive evidence that that resulting morphology is a consequence of extended-chain backbones acting as sites for nucleation of chain-folded growth in directions perpendicular to the extended-chain crystal structure.

This paper describes the crystalline morphology induced in linear polyethylene when it is crystallized under the simultaneous influence of flow orientation and high pressure realized in the Instron capillary rheometer. The pressure and orientation effects resulted in an unusually transparent high density polyethylene having a significant content of highly oriented crystallites.<sup>12-14</sup> The resulting highly ordered, fibrous texture was observed to have many similarities to morphologies generated in shear-crystallized, high-pressure-crystallized, and cold-drawn polyethylene.

### EXPERIMENTAL

The polymer used in this study was commercially available high-density polyethylene, Dupont Alathon 7050, having number- and weight-average molecular weights of 18,400 and 52,500, respectively. Samples were prepared in the Instron rheometer operated at a constant plunger velocity by using a capillary 0.0508 cm in diameter and 1.55 cm long with a 90° entrance angle. Crystallization was induced under the combined orientation and pressure effects produced at a 0.5 cm/min plunger velocity and a rheometer temperature of 136°C.

After the plunger was activated, a sustained pressure rise was observed (see Fig. 1), together with abnormal extrudate swelling. Both factors were evidence of crystallite formation. Crystallite nucleation and growth were expected, since the equation of state developed by Wunderlich<sup>1</sup> for high-density polyethylene indicated that the melt was definitely in a supercooled state under the existing pressure and temperature. An observed decrease in the linear extrusion velocity, attributed to crystallization, was accompanied by a rapid increase in the pressure to the 1920 atm upper limit available in the Instron rheometer. The pressure trace (Fig. 1) showed a distinct discontinuity at 575 atm which occurred after crystallization had begun. This inflection point implied that crystallization had resulted in a significant contraction of the polyethylene in the reservoir. Plunger motion was halted at 1920 atm, but extrusion was continued at 0.02 cm/min by adjusting pressure.<sup>13</sup> The distinctive sample morphology discussed herein resulted from the intense orientation effects that occurred as the crystallizing polyethylene was forced under 1920 atm from the cylindrical reservoir of 0.9530 cm diameter into the 0.0508 cm capillary. The partially crystalline mass was subjected to high shear as well as pressure, leading to crystal reorganization as well as additional crystallization. The higher crystalline content was confirmed by the increased heat of fusion of the transparent strands obtained from the capillary relative to that of the polyethylene obtained from the reservoir.<sup>12</sup> The specimens were removed from the rheometer after cooling to 114°C under 1920 atm. This cooling cycle

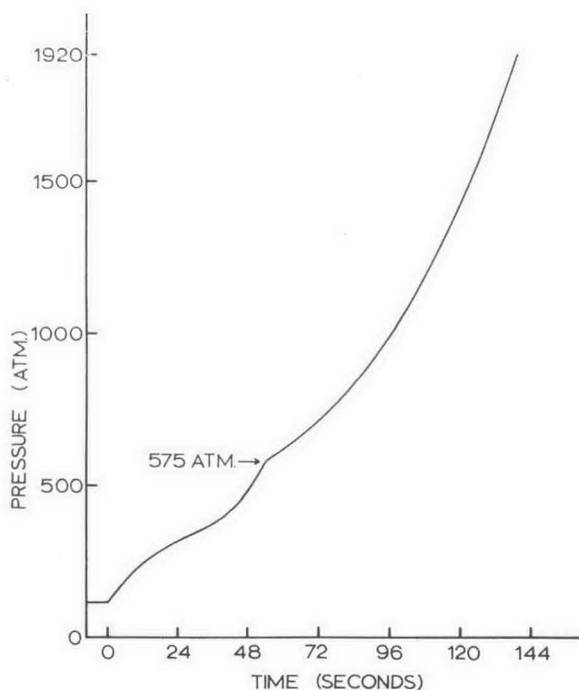


Fig. 1. Instron pressure trace at 136°C under a plunger velocity of 0.5 cm/min with a capillary of 0.0508 cm diameter, 1.55 cm length, and 90° entrance angle.

circumvented the melting that would have occurred at 136°C and atmospheric pressure.

Specimens were examined by scanning electron microscopy (SEM) as well as by direct transmission and replication electron microscopy (TEM). SEM specimens were prepared by fracturing the transparent strands longitudinally, vacuum-coating with 50 Å gold film, and then observing with a Cambridge Ultrascan instrument. TEM specimens were prepared using such techniques as one-step and two-step replication methods, ultramicrotomy with Br<sub>2</sub> staining, and selected-area electron diffraction. A Phillips EM 200 electron microscope equipped with a tilting stage and a Jeolco T7 electron microscope were used to observe the TEM specimens. Preparation and observational procedures will be further discussed as necessary in conjunction with specific micrographs.

## RESULTS

### Sample Appearance

The transparent strands were formed by a procedure that was similar to a drawing operation. In light of Peterlin's observation that extensive drawing causes localized melting during deformation,<sup>15</sup> it was anticipated that the restructured extruded strands would have a morphology different

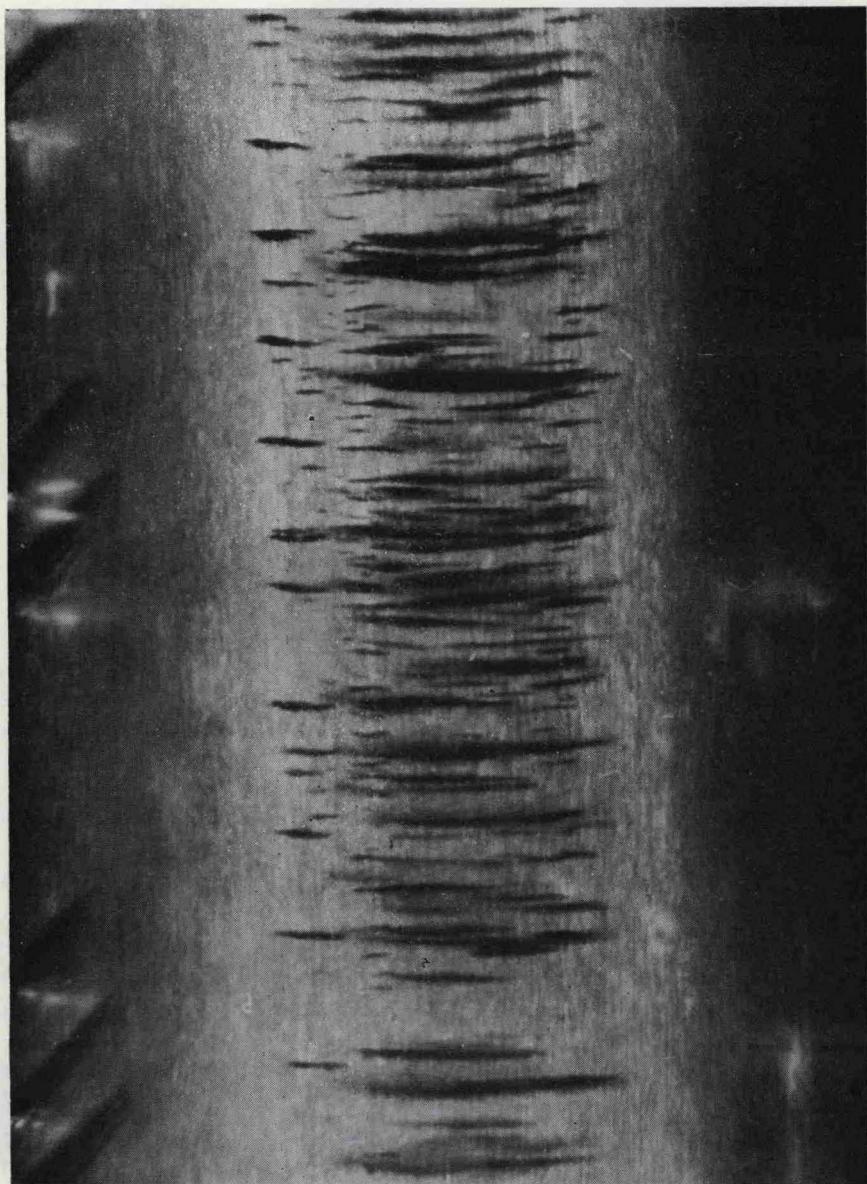


Fig. 2. Microcracks in a strand crystallized in the Instron rheometer at 131°C (optical micrograph).

than that of the polyethylene obtained from the reservoir. Furthermore, the transparent strands were not simply the result of crystallization directly from the flowing melt in the capillary. Indeed, transparent strands were also formed at 60°C by simply applying 1920 atm to a solid plug of polyethylene in the reservoir, forcing it into the capillary to form the unusual structure of the strand. However, the lower-temperature procedure often resulted

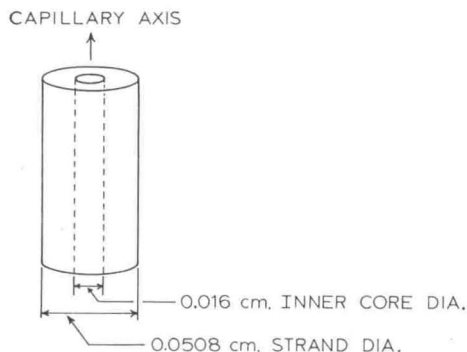


Fig. 3. Schematic diagram of strand indicating inner and outer sheaths discussed in the text.

in microcracks located mainly in the central core of the strands (see Fig. 2). The fusion curve for the sample shown in Figure 2 was both lower and broader in melting temperatures than curves for samples crystallized at  $136^{\circ}\text{C}$ .<sup>13</sup> The existence of microcracks running both perpendicular to the strand length and at  $45^{\circ}$ , together with the observed lower melting point, were consistent with the disruption of the crystalline structure due to excessive stress. The central core structure failed under tensile stress, as is indicated by the cracks in the region perpendicular to the strand length; the structure failed in shear near the outer radius, as is indicated by cracks oriented at  $45^{\circ}$  to the tensile force (the maximum-shear plane). This was consistent with a previous observation that the maximum longitudinal velocity gradient responsible for drawing occurs along the central axis of the strand, while the maximum radial velocity gradient, a shearing effect, occurs near the outer radius.<sup>12</sup> Morphological observations described in this paper indicate basic structural differences between the inner core and the outer sheath of the strand which are defined schematically in Figure 3. In all probability, these differences arise from the different orientation effects attributed to the different velocity gradients existing in the central core and the outer sheath regions during the crystallization process.

### Scanning Electron Microscopy

In spite of the  $200 \text{ \AA}$  resolution limit of the SEM, its large depth of field proved to be invaluable in defining the structure. Two distinct fibrous textures were observed. One of these, shown in Figure 4, was found only in the outer sheath of the strand. These  $3000 \text{ \AA}$  diameter fibers, oriented parallel to the flow direction, formed the dominant structure for radius values  $0.008\text{--}0.025 \text{ cm}$  delineating the outer sheath (see Fig. 3). A cross texture running perpendicular to the  $3000 \text{ \AA}$  diameter fiber axes was observed upon close inspection of Figure 4. This texture appeared to be spaced more or less periodically along the main fibers at  $500 \text{ \AA}$  intervals and often spanned several adjacent fibers. The cross texture appeared to be

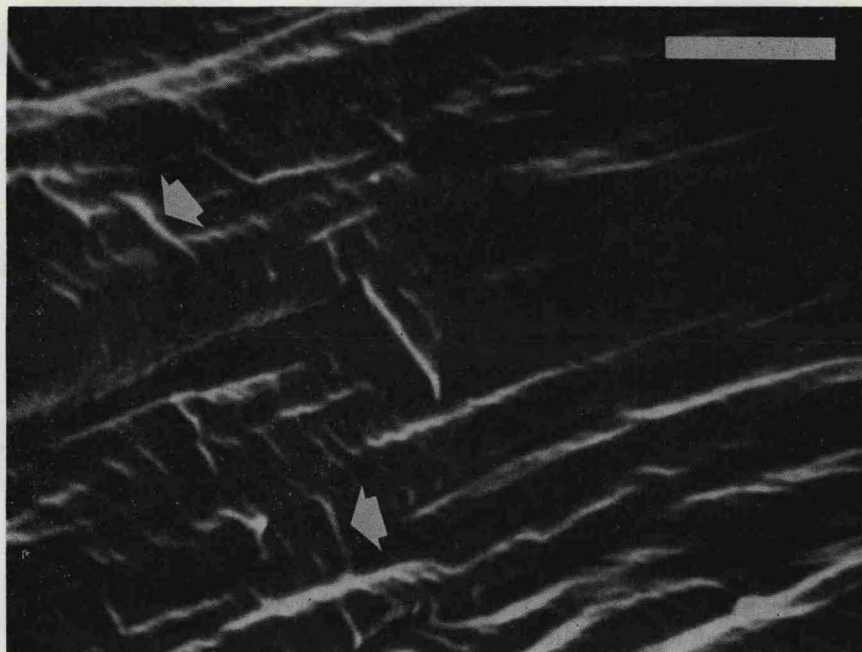
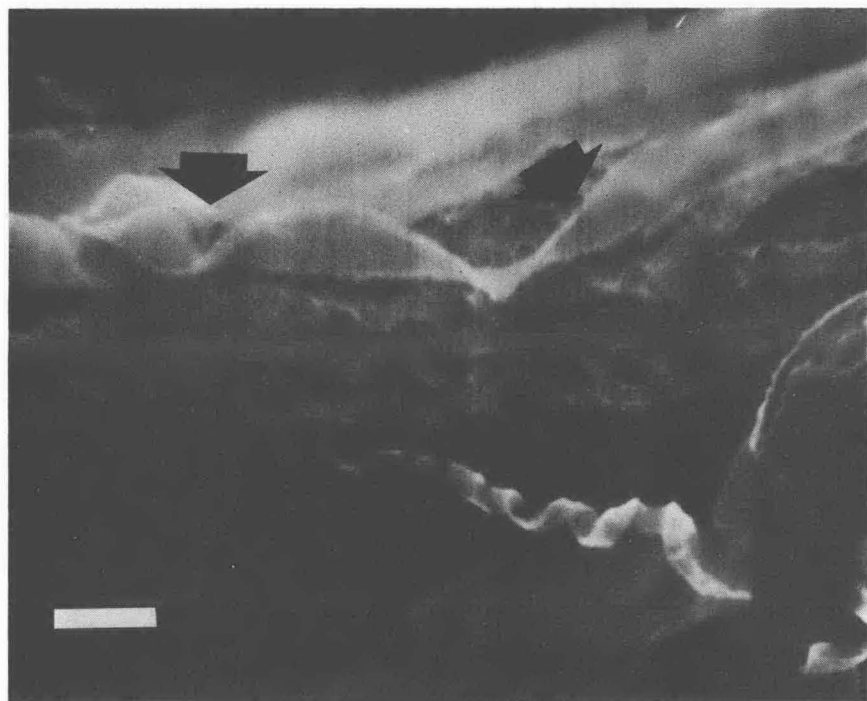


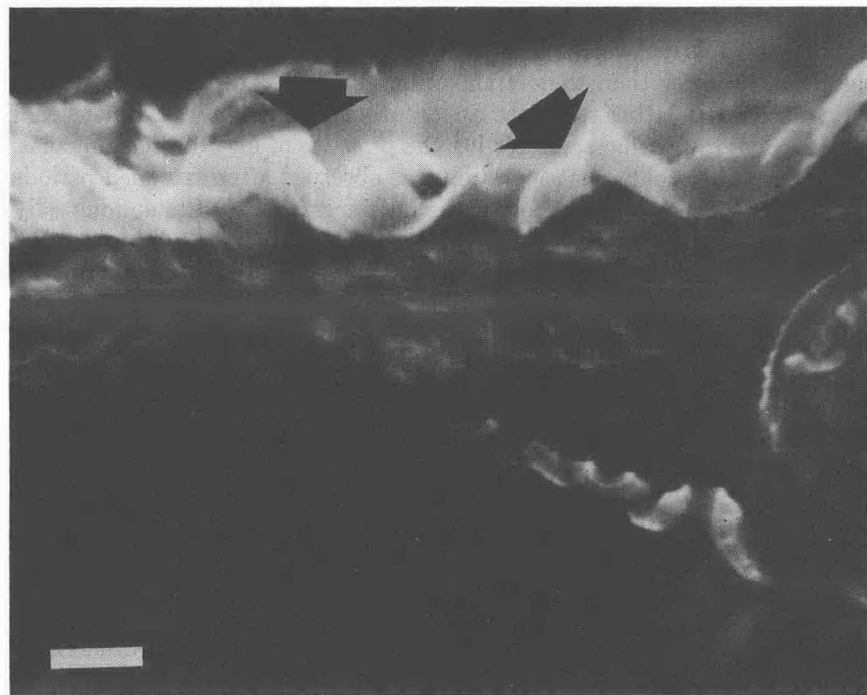
Fig. 4. Outer-sheath texture. Scanning electron micrograph; bar, 1  $\mu$ .

basically lamellar; however, the SEM resolution limit was approached in attempting to further define the texture. In many cases, this lamellar texture was observed to twist around the central fiber thread in a helical fashion. Both the size and orientation of the fibers were consistent with the previously published observations<sup>12</sup> concerning the scanning electron micrograph of a sample fractured by the bending at liquid nitrogen temperatures.

The inner core of the strand consisted of fine, flat, ribbonlike structures, rather than the 3000 Å diameter fibers comprising the outer sheath. When freshly cleaved samples were first introduced into the SEM, the ribbons appeared to be flat and aligned parallel to one another as well as to the capillary axis (Fig. 5a). After approximately 30 min, these ribbons began to move apart and coil into a twisted array. This effect is illustrated by comparing the structures (note arrows) in Figures 5a and 5b, two photomicrographs taken at 10-min intervals. The coiling is not caused by localized heating induced by the electron beam of the SEM because beam energy is far lower than in the conventional electron microscope. Indeed, coiling of fibers exposed by fracture was noted in samples "aged" outside the instrument at room temperature. The higher magnification photomicrograph in Figure 6 shows the separate ribbons curling away from larger ribbon bundles (note arrows). Regular cross striations were also observed on the inner core ribbons; however, this particular cross texture appeared to resemble a crystallographic pleating rather than a lamellar overgrowth. The individual ribbons varied in approximate width between 1000 and 5000 Å and were estimated to be approximately 200–400 Å thick. The



(a)



(b)

Fig. 5. Inner-core texture: (a) upon insertion into the microscope; (b) 10 min after insertion. Scanning electron micrographs: bar,  $1\mu$ .

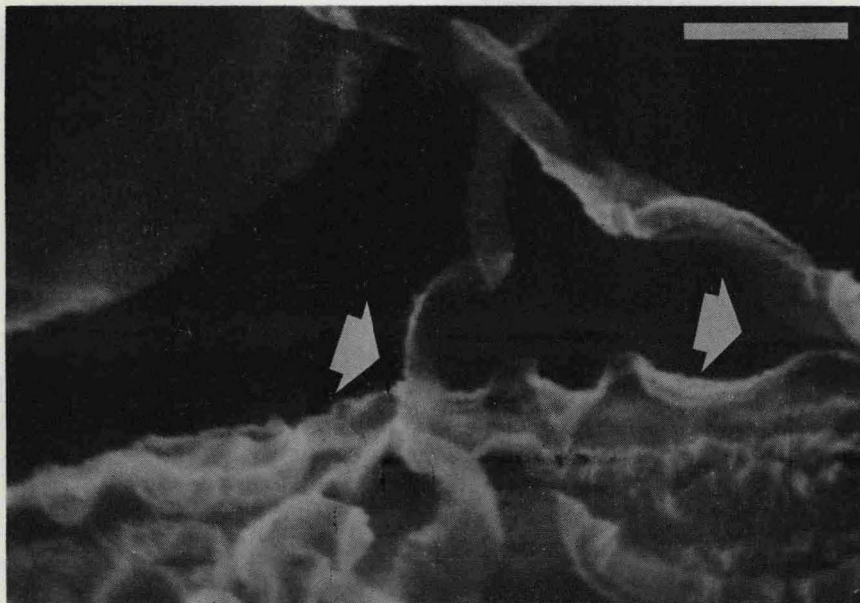


Fig. 6. Ribbons in the inner core. Scanning electron micrograph; bar, 1 $\mu$ .

ribbon substructure will be described in connection with TEM since the thickness measurements approach the SEM resolution limit.

It should be mentioned that the ribbon coiling implies two important features of this particular morphology. First, inter-ribbon bonding is significantly lower than that of the outer sheath. The cross texture observed with the latter structure apparently imparts a three dimensional cohesiveness to the fibers, suggesting the presence of interfibrillar linkages. Indeed, no fiber coiling or separation was observed after extended periods in the SEM. Second, the ribbons in the bulk-crystallized state undoubtedly contained a significant residual strain which is apparently relieved by the coiling mechanism. Such residual strain may have had inherent crystallographic as well as shear-induced origins similar to those causing periodic twisting in polyethylene spherulites.<sup>16</sup>

### Transmission Electron Microscopy

Specimens were examined in the conventional electron microscope using both fracture replication and direct transmission techniques. Fracture-surface replication proved somewhat difficult because of surface roughness. However, good quality replicas were obtained by shadowing the surface directly with Pt-C, evaporating a thin carbon layer, and finally stripping the layers with acetone-swollen acetate strips. The acetate was then removed by dissolving in amyl acetate, to leave a negative Pt-C shadowed carbon replica. Selected-area electron diffraction was performed on several polyethylene fiber fragments which fortunately adhered to such replicas.



Fig. 7. Carbon replica showing inner core fiber bundles. Electron micrograph.

The ribbonlike fibrous texture of the inner core seen in the SEM photomicrographs was also observed in the shadowed carbon replicas. Electron micrographs showed that the ribbons extended for tens of microns and contained fine fiber bundles oriented parallel to the long axis of the strand. Figure 7 is a replication electron micrograph of these fiber bundles, in which parting of the individual fibers from the bundles during fracture replication is visible (see arrows). Note both the fiber lengths and apparently weak interfiber bonding. Individual fiber bundles in microtomed sections were examined by staining with  $\text{Br}_2$  vapor, which preferentially attacks the less ordered regions between the component fibers. Specimens were mounted in an epoxy embedding material (Cargille NYSEM) and sectioned on a Sorvall Porter-Blum MT-2 ultramicrotome by use of a Dupont  $43^\circ$  diamond knife. Sectioning across a strand proved impractical since the fiber bundles readily splayed apart owing to the weak bonding between the fiber bundles. Sectioning parallel to the strand axis proved to be more feasible, but stringy, rather than smooth, sections were obtained with this procedure. Figure 8 is a transmission electron micrograph of microtomed fibers from the strand inner core stained with  $\text{Br}_2$ . The fibrous, stringy texture was quite visible; however, fiber splaying due to the action of the knife was also obvious. The ultimate subunit of the ribbon structure was found to be a 200–250 Å diameter fiber (see arrows in Fig. 8). Since individual fibers adhered to several of their neighbors after splaying apart, some type of interfiber bonding may have existed within a fiber bundle. A nodular structure superimposed on the ultimate fibers was also observed; however, this was probably an artifact of the  $\text{Br}_2$  vapor staining process.



Fig. 8. Microtomed,  $\text{Br}_2$ -stained section from the inner core. Transmission electron micrograph.

### Electron Diffraction

Unstained sectioned fibers and, in a few cases, shadowed fibers adhering to the carbon replicas were examined by electron diffraction using electron microscope stage tilting techniques. Exceptionally well-developed spot patterns were obtained from the strand inner core where the ribbon like structure was observed. Proper stage rotation revealed a highly ordered and oriented crystal structure within the ultimate fibers. Figures 9 and 10 show sharp electron diffraction patterns and the corresponding reciprocal lattice diagrams obtained from the inner core material. Note that the shorter exposure time of Figure 9 permitted observation of lower-order reflections, whereas the longer exposure time of Figure 10 provided the higher-order reflections. In both cases,  $(0kl)$  reflections were observed while  $(h0l)$  reflections were undetectable with further stage rotation. No explanation was found for the failure to detect the  $(h0l)$  reflections, other than thickness effects associated with difficulty in passing electrons through the thick dimension of the ribbon. This would suggest that interfiber bonding in ribbons occurs primarily along  $(0k0)$  planes.

The polyethylene crystal structure is based on an orthorhombic unit cell, requiring that the reciprocal and true lattice directions be parallel. Furthermore, polyethylene belongs to the  $D_{2h}^{16}$  space group. Such symmetry conditions require that permissible  $(0kl)$  reflections satisfy the equation:  $k + l = 2n$ . Each of the twenty-six distinct reflections observable in

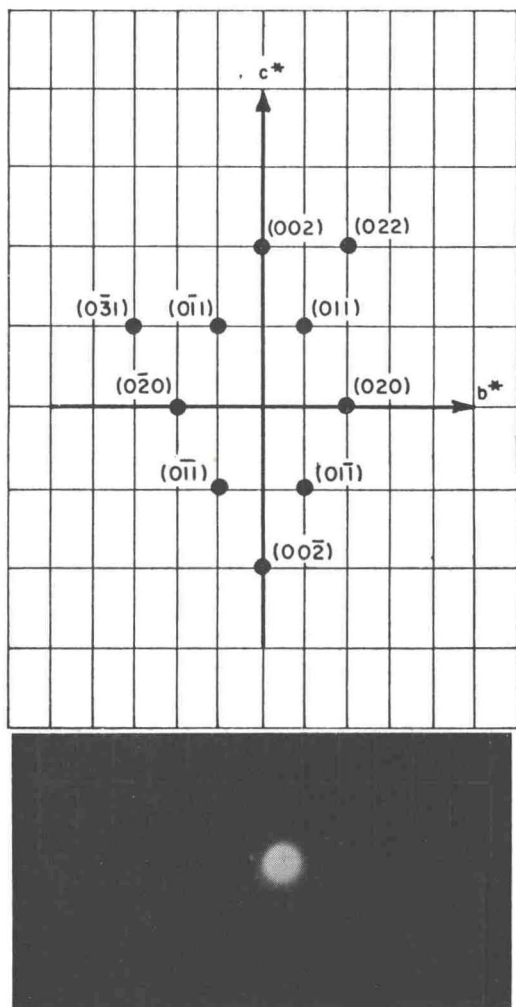


Fig.9. Electron diffraction pattern and reciprocal lattice diagram of inner-core material.

Figures 9 and 10 comply with this restriction. The electron diffraction data show that an unusually high degree of crystalline order (for polyethylene) exists in the inner core of the strand. The crystallographic  $c$  axis, the axis parallel to the polyethylene chain backbone, was found to be oriented parallel to the long axis (within  $\pm 5^\circ$ ) of the strand. This high degree of chain orientation is consistent with the  $c$ -axis orientation function  $+0.996$  determined previously with wide-angle x-ray measurements.<sup>14</sup> In contrast, electron diffraction studies of the 3000 Å diameter, fibrous morphology of the outer sheath produced only typical oriented fiber patterns similar to those obtained by Keller<sup>10,11</sup> from stress-crystallized polyethylene. The resulting diffuse arcs may have been produced by the polycrystalline lamellar cross texture observed on the 3000 Å fibers.

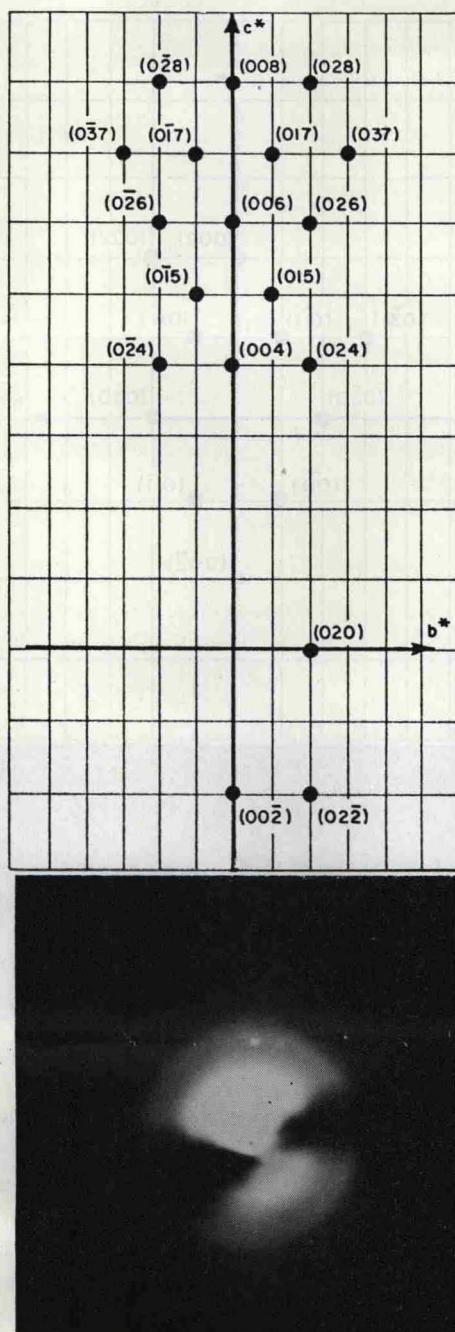


Fig. 10. Electron diffraction pattern and reciprocal lattice diagram of inner-core material (long exposure time).

## DISCUSSION AND CONCLUSIONS

Two distinct morphological units are produced in the Instron strands: the highly crystalline ribbons in the inner core and the less ordered 3000 Å diameter fibers of the outer sheath. Similar units have been observed by Pennings and Kiel<sup>7</sup> in the fibrous structures crystallized under the influence of shear in a dilute solution. They, too, described the morphological entities as being either ribbons or fibers having a lamellar overgrowth. The 3000 Å fibers may well be the melt-crystallized analog of the fibers grown from dilute solution by Pennings and Kiel.

Fibrous morphologies are not uncommon in crystalline polymers, especially if the polymer chain backbone is too stiff to accommodate chain folding. O'Leary and Geil<sup>17</sup> have described the fibrous textures in crystalline polytetrafluoroethylene in a manner similar to that used to define the polyethylene structure of this work. Crystal<sup>18</sup> has also described a fibrous morphology for crystalline poly-*N*-vinyl-carbazole, an apparently stiff molecule containing bulky pendant groups which inhibit free rotation about the polymer backbone. Because chain folding cannot be accommodated in poly-*N*-vinylcarbazole, this polymer apparently crystallizes into a fibrous structure containing weak interfiber bonds. While *c*-axis orientations were noted in these references, sharp-spot electron diffraction patterns were not reported.

Additional evidence for the existence of two distinct morphological units in the Instron strands was found in the fusion curves obtained from the melting of the strands in the Perkin-Elmer differential scanning calorimeter (DSC), Model 1-b. The DSC traces for two strands crystallized with the Instron procedure at 132°C are shown in Figure 11. It was noted that these strands appeared to be similar in structure to those examined in the above micrographs (crystallization at 136°C). One of the strands was exposed to 25 Mrad of irradiation in order to suppress reorganization during melting.<sup>19,20</sup> Both strands were found to have relatively high peak-value melting points, consistent with the presence of extended-chain crystals.<sup>4</sup> Furthermore, the irradiated strand showed a multipeak fusion curve indicative of two crystalline forms. A possible explanation for such behavior would be that the more perfect inner-core ribbon structure melted at the higher peak temperature, and the less ordered outer-sheath structure, containing chain-folded lamellae and defects, melted at the lower peak temperature. The primary effect of the radiation has been to resolve the single fusion curve, corresponding to the unirradiated sample, into low and high melting peaks for the irradiated sample. These observations are consistent with the hypothesis that the structure in the inner core of the strand appears to be dominated by an extended-chain crystalline structure, while that of the outer sheath is dominated by epitaxial chain-folded lamellae.

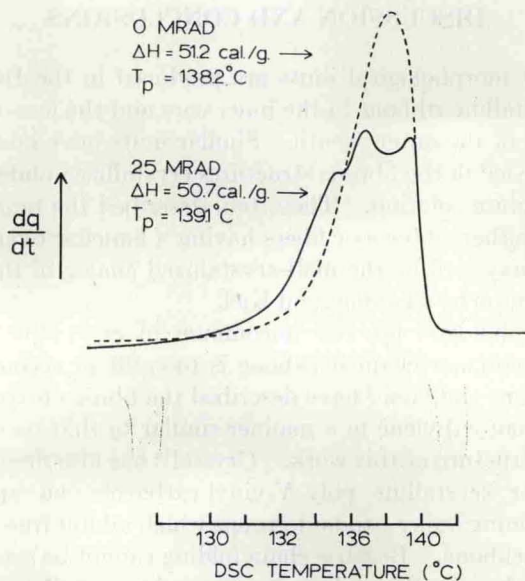


Fig. 11. Differential scanning calorimeter trace showing the effect of irradiation on the melting behavior of a transparent strand, produced at  $132^\circ\text{C}$  with a capillary of diameter 0.0762 cm and 1.0 cm/min plunger velocity.

The inner-core ribbon structure was the most perfect of the two crystalline units defined in this study. Well developed single-crystal electron diffraction patterns obtained from ribbons indicate that they are made up of extended-chain crystals. The eighth-order reflection along the  $c$  axis has been detected (see Fig. 10) by using a very small aperture achieved with the Phillips EM200 knife-type diffraction aperture. In order to obtain such an electron diffraction pattern, the crystalline order must have been in register over a considerable portion of the aperture opening. Otherwise, a more polycrystalline pattern would be expected. Note that a lamellar structure connected by tie molecules, such as the model proposed by Peterlin for drawn polyethylene,<sup>15</sup> would not result in sharp diffraction spots for the  $(0kl)$  planes over a 5000 Å length of the fiber. In the Peterlin model, the lamellae that stack together to form a fibril would be free to rotate around the  $c$  axis, thereby prohibiting the formation of coherent sets of diffraction planes for all except the  $(00l)$  planes. Figures 9 and 10 show the presence of other sets of diffraction planes. Only a well developed extended-chain crystal model which maintains a high degree of order and register across the aperture opening could account for the observed diffraction spots from the inner-core fibers.

The formation of an extended-chain structure by crystallizing from the bulk polyethylene is particularly significant from the aspect of improved mechanical properties. In addition to the transparency of the strands, the modulus of the central core containing the extended-chain crystal structure may well be extremely high in the direction of the strand length. If defect-

free extended-chain ribbons could be produced in a commercial process analogous to the Instron procedure, significant improvement in mechanical properties would be realized.

The authors wish to thank F. J. Walton and R. Fernquist of the Xerox Corporation for their invaluable technical assistance throughout this project. The authors are also indebted to P. Goldstein of the Xerox Corporation and R. S. Porter, R. S. Stein, F. P. Price, and R. D. Ulrich of the University of Massachusetts for helpful discussions.

### References

1. B. Wunderlich and T. Arakawa, *J. Polym. Sci. A*, **2**, 3697 (1964).
2. E. Hellmuth and B. Wunderlich, *J. Appl. Phys.*, **36**, 3039 (1965).
3. B. Wunderlich and C. Cormier, *J. Polym. Sci. A-2*, **5**, 987 (1967).
4. D. Rees and D. Bassett, *J. Polym. Sci. B*, **7**, 273 (1969).
5. L. Mandelkern, M. Gopalan, and J. Jackson, *J. Polym. Sci. B*, **5**, 1 (1967).
6. B. Wunderlich, *J. Polym. Sci. B*, **5**, 7 (1967).
7. A. Pennings and A. Kiel, *Kolloid-Z. Z. Polym.*, **205**, 160 (1965).
8. T. Kawai, T. Matsumoto, M. Kato, and H. Maeda, *Kolloid-Z. Z. Polym.*, **222**, 1 (1969).
9. R. Williamson and R. Novak, *J. Polym. Sci. B*, **5**, 147 (1967).
10. M. Hill and A. Keller, *J. Macromol. Sci.-Phys.*, **B3**, 153 (1969).
11. A. Keller, *Repts. Progr. Phys.*, **31**, 623 (1968).
12. J. H. Southern and R. S. Porter, *J. Macromol. Sci.-Phys.*, **B4**, 541 (1970).
13. J. H. Southern and R. S. Porter, *J. Appl. Polym. Sci.*, **14**, 2305 (1970).
14. C. R. Desper, J. H. Southern, R. D. Ulrich, and R. S. Porter, *J. Appl. Phys.*, **41**, 4284 (1970).
15. A. Peterlin, *Polym. Eng. Sci.*, **9**, 172 (1969).
16. J. R. Burns, *J. Polym. Sci. A-2*, **7**, 593 (1969).
17. K. O'Leary and P. H. Geil, *J. Appl. Phys.*, **38**, 4169 (1967).
18. R. G. Crystal, paper presented to the Division of High Polymer Physics, American Physical Society Meeting, Dallas, Texas, March 1970; *Macromolecules*, in press.
19. H. E. Bair and R. Salovey, *J. Macromol. Sci.-Phys.*, **B3**, 3 (1969).
20. T. W. Huseby and H. E. Bair, *J. Polym. Sci. B*, **5**, 265 (1967).

Received October 27, 1970

Revised March 15, 1971